Carrier Separation at Dislocation Pairs in CdTe

Chen Li,[1,2] Yelong Wu,[3] Timothy J. Pennycook,[1,4,*] Andrew R. Lupini,[1] Donovan N. Leonard,[1] Wanjian Yin,[3] Naba Paudel,[3] Mowafak Al-Jassim,[5] Yanfa Yan,[3] and Stephen J. Pennycook[1,†]

[1]*Materials Science and Technology Division, Oak Ridge National Laboratory, Oak Ridge, Tennessee 37831, USA*
[2]*Department of Chemistry, Vanderbilt University, Nashville, Tennessee 37235, USA*
[3]*Department of Physics and Astronomy, The University of Toledo, Toledo, Ohio 43606, USA*
[4]*Department of Physics and Astronomy, Vanderbilt University, Nashville, Tennessee 37235, USA*
[5]*The Measurements and Characterization Group, National Renewable Energy Laboratory, Golden, Colorado 80401, USA*

(Received 20 May 2013; published 29 August 2013)

Through the use of aberration corrected scanning transmission electron microscopy, the atomic configuration of CdTe intragrain Shockley partial dislocation pairs has been determined: Single Cd and Te columns are present at opposite ends of both intrinsic and extrinsic stacking faults. These columns have threefold and fivefold coordination, indicating the presence of dangling bonds. Counterintuitively, density-functional theory calculations show that these dislocation cores do not act as recombination centers; instead, they lead to local band bending that separates electrons and holes and reduces undesirable carrier recombination.

DOI: 10.1103/PhysRevLett.111.096403 PACS numbers: 71.20.Nr, 68.37.Ma, 73.50.Gr, 88.40.jm

Cadmium telluride (CdTe) is a II-VI compound semiconductor that is considered a near perfect material for low-cost high-efficiency thin-film solar cell applications [1,2]. Its direct band gap of $\sim$1.48 eV gives a nearly optimized absorption region for the solar spectrum and a Shockley-Queisser efficiency limit of $\sim$32% [3,4]. Recent developments have significantly advanced CdTe thin-film solar cell technology and the record efficiency of laboratory CdTe cells has reached 19.6% [5–8].

However, there is still a considerable gap between the current best research cell and the theoretical maximum efficiency. One of the main factors that limits the efficiency of CdTe cells is the low average minority carrier lifetime, usually attributed to nonradiative recombination at grain boundaries (GB) and point defects. Understanding the structure and the behavior of such defects in elemental and compound semiconductors has attracted great attention for a considerable time. In Si, GBs are typically found to be electrically active [9,10]. In contrast, several groups have reported the successful passivation of GBs in $CuInSe_2$ (CIS), $Cu(In, Ga)Se_2$, and CdTe [11–24]. An alternative cause for low efficiency in CdTe could be carrier recombination at *intragrain* defects, which are common due to the low stacking fault energy [25]. However, the electrical activity of intragrain partial dislocations in CdTe has not previously been determined. In silicon, calculations of reconstructed 30° partial dislocations have found them to be electrically benign [26], whereas in III/V semiconductors electrically active states were found in the band gap [27,28]. Therefore it seems entirely plausible that intragrain dislocations in CdTe, also a compound semiconductor, may have electrically active gap states that limit the device efficiency.

Direct determination of dislocation core structures by transmission electron microscopy (TEM) was very challenging prior to aberration correction [29]. In the present work we have used state of the art aberration-corrected scanning transmission electron microscopy (STEM) with sub-Å resolution to determine the atomic structures of intragrain defects in CdTe. STEM Z-contrast images are sensitive to the atomic number of the elements [30,31], which enables us to distinguish Cd and Te atomic columns directly from the image intensity, resolve the lattice polarity, and further determine the core configurations of Shockley partial dislocations. Structure models derived from the STEM images have been constructed and relaxed by density-functional theory (DFT) calculations. The relaxed structures are found to be in good agreement with the experimental images. The corresponding band structures indicate that the Shockley partial dislocation pairs are *not* electrically active. Furthermore, we find that charge transfer between the Te core (a shallow acceptor) and the Cd core (a shallow donor) causes significant band bending, which would actually help to keep the electron-hole pairs separated.

The CdTe solar cells studied for the present work have a structure of $CdTe/CdS/SnO_2$:F/glass. The CdTe layers, with a thickness of 4 μm, were grown by close-space sublimation and the CdS layers of about 100 nm thick were grown by rf sputtering on SnO_2:F coated commercial soda lime glass substrates. Both focused ion beam and conventional polishing and ion milling techniques have been used to prepare CdTe samples for microscopic study. Atomic resolution STEM images were acquired with Nion UltraSTEM 100 and 200 microscopes [32]. The DFT structural optimizations and energy band calculations were performed using the local density approximation with the Hubbard U correction (LDA + U) method [33,34]. The LDA + U functional is adapted from the

 © 2013 American Physical Society

formalism of Ref. [35] with a U value of 7 eV, which gives good predictions for the structural and electronic properties of CdTe [36]. The projector augmented wave method [37] as implemented in the VASP code [38,39] was employed. The energy cutoff was set at 350 eV and a $6 \times 1 \times 1$ k-point grid was used for structural optimizations. The calculated equilibrium lattice constant of bulk CdTe is 6.40 Å, which is quite close to the experimental value of 6.48 Å [40]. Cd ($4d$, $5s$) and Te ($5s$, $5p$) were treated as valence states. The calculated band gap for bulk CdTe is 0.98 eV, while the experimental value is about 1.5 eV [41]. Band alignment of the different structures is determined by comparing calculated core levels.

Z-contrast images in Fig. 1 show the atomic configuration of several dislocations observed within CdTe grains along the $\langle 110 \rangle$ direction. As Te is slightly heavier than Cd, in the perfect crystal we are able to distinguish the columns from their image intensities [42]. Since the intensity of the columns in the dislocation cores could be affected by the presence of vacancies, strain, etc., we identify the polarity in the dislocation core based on their bonding to surrounding columns. In Fig. 1, the small blue and large yellow circles indicate Cd and Te columns, while the white boxes in Figs. 1(a) and 1(b) indicate intrinsic and extrinsic stacking faults, respectively. If one close-packed plane is removed from perfect CdTe, which has a zinc blende structure, an intrinsic stacking fault is formed. If an extra plane is inserted, an extrinsic stacking fault is created. Those stacking faults, as well as twin boundaries, are very common planar defects within CdTe grains. It is seen that when the stacking faults terminate into perfect crystal, instead of Cd-Te dumbbells, unpaired Cd and Te atomic columns appear at the partial dislocation cores. In Fig. 1(a), there are two partial dislocation cores, one at each end of the intrinsic stacking fault. One partial contains a single Cd column and the other contains a single Te column. We refer to these partials as a Cd core and a Te core, respectively. This kind of glide set partial dislocations is associated with slip, and a Burgers vector analysis indicates that the angle of the dislocation line and the Burgers vector is 30° [42]; therefore, they are 30° Shockley partial dislocations. Figure 1(b) shows a 90° Shockley partial dislocation at the end of an extrinsic stacking fault. Two unpaired Te columns are indicated with large yellow circles in the Te-partial core. The corresponding Cd-partial core with two unpaired Cd columns is often found at the other end of the stacking fault, as we have reported previously [42]. The unpaired Cd and Te columns in the dislocation cores suggest the presence of dangling bonds, which often introduce states inside the band gap, and facilitate nonradiative recombination.

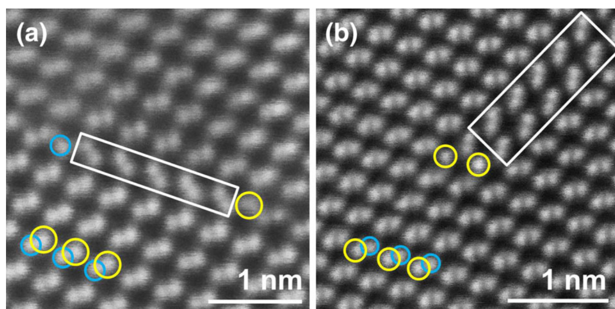

FIG. 1 (color online). Z-contrast images showing (a) Cd and Te unpaired atomic columns at a pair of partial dislocations at the two ends of an intrinsic stacking fault and (b) Two unpaired Te columns at a partial dislocation at the end of an extrinsic stacking fault. Small blue and big yellow circles indicate Cd and Te atoms, respectively. The white boxes indicate stacking faults.

In the thinnest regions of specimen we were able to observe changes in the dislocation structure induced by the beam, which are representative of the atomistic processes of dislocation motion (see Supplemental Material, movie 1 [43]). Figures 2(a)–2(c) show frames extracted from a Z-contrast STEM movie showing the disappearance of an intrinsic stacking fault. The small blue and large yellow circles mark the locations of unpaired Cd and Te atomic columns, respectively, in the dislocation cores. The white rhombohedron indicates the location and length of the intrinsic stacking fault. Between Figs. 2(a) and 2(b), the position of the Cd core at the left side shifted toward the Te core, thus shortening the stacking fault by one dumbbell. After being scanned by the electron beam for a few minutes, the stacking fault became progressively shorter and eventually disappeared, as shown in Fig. 2(c). Figures 2(d)–2(f) are Z-contrast images taken after the movie showing the reappearance and subsequent disappearance of the fault. Scanning this area for another 10 min did not cause the fault to reappear. The fact

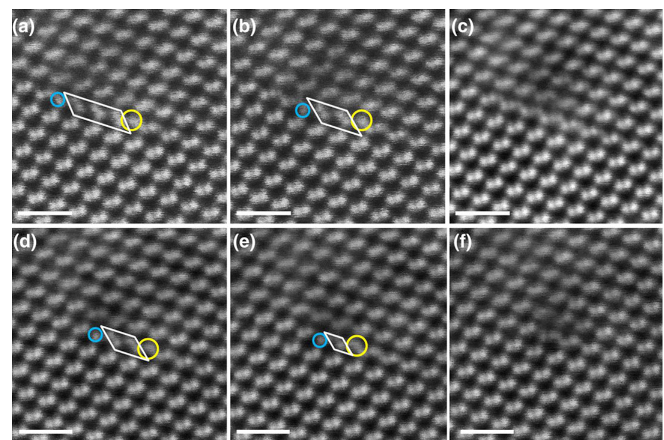

FIG. 2 (color online). (a)–(c) are frames from a Z-contrast STEM movie showing the disappearance of an intrinsic stacking fault. (d)–(f) are Z-contrast images that were taken after the movie, showing the fault reappearing and disappearing again. The small blue and large yellow circles indicate unpaired Cd and Te atomic columns in the dislocation cores, respectively. The white boxes indicate the intrinsic stacking fault. The scale bars are 1 nm.

that the partial dislocation pairs can be created, changed, and removed easily under the beam indicates a low formation energy for this dislocation structure. The mechanism of this beam induced motion is direct momentum transfer (knock-on processes) from the high-energy electron beam to the sample, as has been reported recently in the case of Si_6 clusters [44]. In thicker regions of specimen such motion was reduced, although the same core structures were observed. The density of partial dislocations is higher in the thin areas, suggesting that many dislocations in the thin areas are actually induced by the ion milling used to thin the samples.

To investigate the effect of these intragrain dislocations on the electronic properties of CdTe, structure models were constructed based on the STEM images and relaxed by DFT calculations. The dislocation structures were incorporated into a supercell of 120 atoms consisting of $1 \times 10 \times 6$ primitive unit cells as shown in Figs. 3(a) and 3(b) for the intrinsic and extrinsic stacking faults, respectively. X is the direction along the dislocation line. Y and Z are the directions along and across the fault, respectively. Only the atoms in the dashed boxes were relaxed until the force acting on each atom was less than 0.02 eV/Å. The relaxed structures match well with the experimental images. The minimum energy core structures are not reconstructed into dimers, reflecting the more ionic character of the II/VI materials than the III/V or group IV materials.

The atoms in the Cd1 and Te1 columns in both the intrinsic and extrinsic stacking faults have dangling bonds, possessing a near sp^2 configuration rather than the sp^3 configuration of bulk CdTe. In the $\langle 110 \rangle$ viewing direction, these atoms appear further away from their Te and Cd neighbors than in the perfect dumbbells. In the extrinsic case, atoms in the Cd4 and Te4 columns (in the Te and Cd core, respectively) also have fivefold coordination. Dangling bonds usually create deep levels within the band gaps of semiconductors. A common approach to looking for such defect states is to examine the band structure and density of states (DOS), and these are presented for the intrinsic and extrinsic stacking faults in Figs. 3(c) and 3(d). The energy zero is set to the Fermi level. The band gap calculated for bulk CdTe is 0.98 eV. Given that both partial dislocation structures have states within the energy range of the band gap of bulk CdTe, one might conclude that the partial dislocation pairs create gap states and are electrically active.

However, these "mid-gap" states do not exhibit the characteristics of localized defect states. Instead, they appear rather delocalized, following the curvature of the bands outside the range of the bulk band gap. Furthermore when one examines the band structure of each partial dislocation core individually, it becomes apparent that they do not introduce defect states in the gap. The slab configurations used to examine Cd and Te cores are shown in Fig. 4 for the intrinsic stacking fault and in Fig. S1 of the Supplemental Material [43] for the extrinsic stacking fault. Cd and Te atoms at the surfaces were passivated by pseudo H atoms with atomic numbers $Z = 0.5$ or 1.5. The band structure and DOS of each configuration are shown alongside the structure models in the figures, and again the energy zero is set to the Fermi level. Each structure with only a single dislocation core has a band gap at least as wide as that of bulk CdTe, and in a very similar energy range, with no gap states.

With defect states from the individual cores ruled out, it would seem the states between zero and one eV in the full

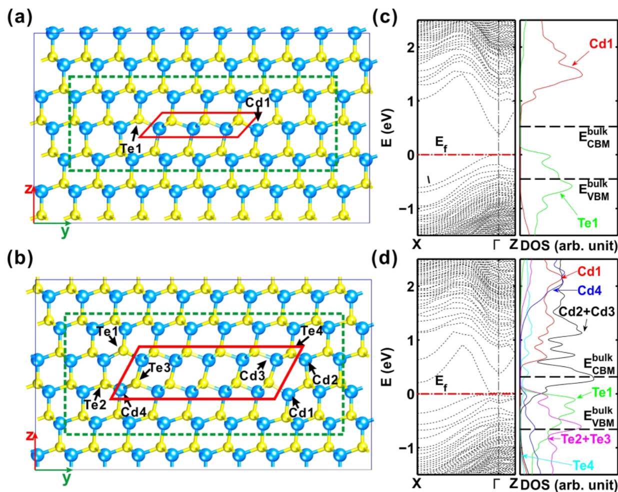

FIG. 3 (color online). Atomic structure models of (a) intrinsic and (b) extrinsic stacking faults. The red boxes indicate the stacking faults. (c) and (d) show the band structure and projected DOS of the partial dislocations at intrinsic and extrinsic stacking faults, respectively. A large density of states appears in the band gap. The energy zero is set to the Fermi level of the stacking fault. X is the direction along the dislocation line. Y and Z are the directions along and across the fault, respectively.

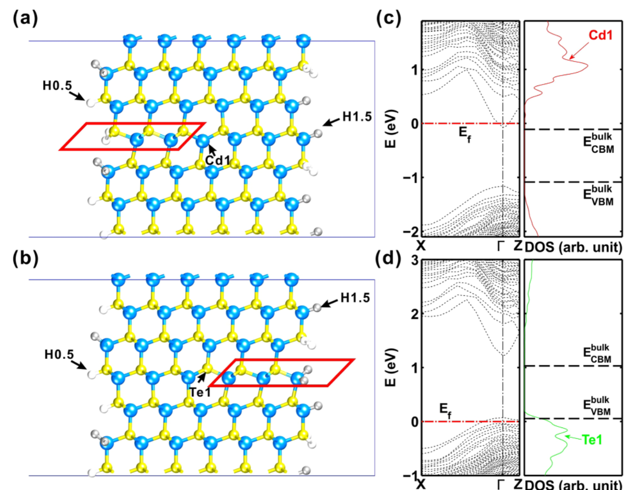

FIG. 4 (color online). Supercells containing (a) an individual Cd core and (b) an individual Te core of an intrinsic stacking fault. The red boxes indicate the intrinsic stacking fault. Band structure and DOS of individual cores: (c) Cd core; (d) Te core. No gap states are found.

stacking fault structures must originate from some interaction between the cores. Further examination of the electronic structure of the individual dislocation cores reveals that the Cd dislocations act as shallow donors while the Te cores act as shallow acceptors, as indicated by the Fermi levels in the band structure diagrams. When the Cd and Te cores are paired together, the extra electron from the Cd core fills the hole provided by the Te core. The transfer of an electron from the Cd core state to the Te core state suggests the possibility of a dipole between the cores. The possibility of such a charge gradient between 30° and 90° partial pairs has been suggested previously in GaAs [28].

To investigate the extent of charge transfer between the two cores, in Fig. 5(a), we plot the probability densities of the highest occupied (red) and the lowest unoccupied (green) states shown in Fig. 3(c). Unlike localized defect states, they are seen to be delocalized, extending across many dumbbells away from the dislocation cores, consistent with their identification as energy bands of the crystal. However, the highest regions of probability density of the two states are segregated in the direction separating the two cores. The probability density of the highest occupied state is more highly concentrated around the Te core, while that of the lowest unoccupied states is more concentrated around the Cd core, demonstrating that the extra electron from the Cd core transfers to the Te core region. However, this does not rule out the possibility of other electrons moving to the Te core region to compensate the resulting charge imbalance.

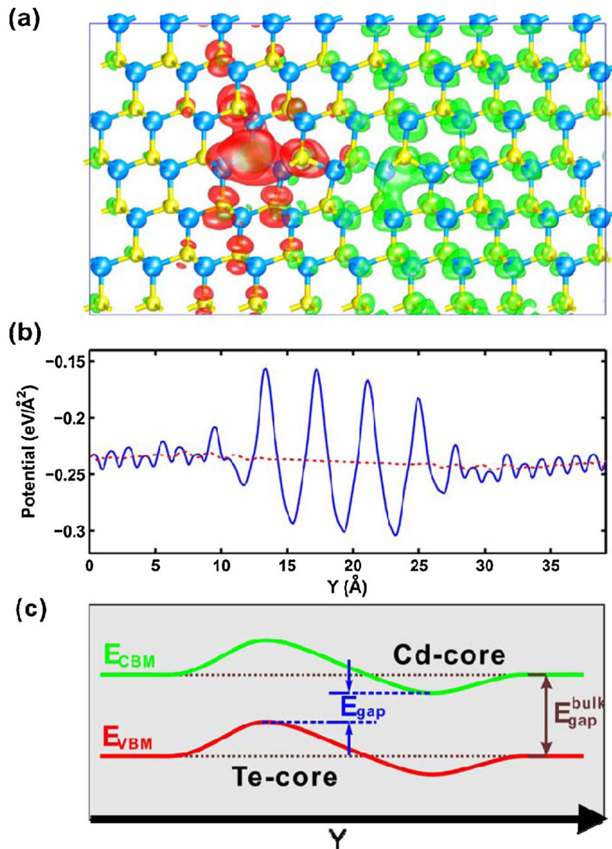

FIG. 5 (color online). (a) Calculated probability densities of the highest occupied (red) and the lowest unoccupied (green) states shown in Fig. 3(c) (isosurface value: 1.5×10^{-3} e/Å^3). (b) The blue line shows the electrostatic potential along the stacking fault, while the red dashed line indicates the average electrostatic potential. Y is the direction along the fault. (c) Schematic showing the band bending caused by the charge transfer between the Te core and the Cd core. E_{gap} indicates the energy difference between the gap states above and below the Fermi level marked in Fig. 3(c).

To determine if a dipole is present between the cores, we plot the electrostatic potential energy along the stacking fault in Fig. 5(b). Though the potential energy oscillates up and down between the cores (blue line), the sliding average (red dotted line) of the potential energy exhibits a continuous downward slope from the Te core to the Cd core, showing that there is indeed a potential difference between them. The electric field resulting from this potential difference will cause the bands to bend as illustrated in Fig. 5(c), increasing in energy around the Te core and decreasing in energy around the Cd core. A similar result is found for the extrinsic stacking fault and is shown in Fig. S2. Such band bending explains the presence of states within the energy range of the bulk band gap seen in Figs. 3(c) and 3(d). The upward shift in energy of the bands at the Te core causes states from the valance band to appear above the valence band maximum (VBM) of bulk CdTe, while the downward shift in energy at the Cd core causes conduction band states to appear below the conduction band minimum (CBM) of the bulk. Because excited electrons fall to the bottom of the conduction band and holes move to the highest available energy in the valance band, such band bending provides greater separation between the electrons and holes, actually reducing the rate of undesirable carrier recombination. This effect may explain the band bending reported at Cu(In, Ga)Se_2 grain boundaries [45,46].

In conclusion, with aberration corrected STEM, single Cd and Te columns have been found at the intragrain Shockley partial dislocation cores where the stacking faults terminate. DFT calculations show these intragrain dislocations do not create states inside the band gap but cause a significant energy band bending, due to the charge transfer between the Te-partial dislocation core and the Cd-partial dislocation core. Since the cores do not introduce gap states, the stacking faults cannot act as recombination centers, and are electrically benign. Moreover, because of the band bending they induce, the dislocation core pairs actually encourage greater separation of the carriers. Thus, counterintuitively, improved cell efficiency may result from *increasing* the density of intragrain stacking faults and partial dislocation pairs. A similar conclusion might apply to other II-VI and III-V compound semiconductors, as they are also likely to have pairs of nonstoichiometric dislocations that behave as shallow acceptors and donors.

The authors are grateful to S. T. Pantelides for helpful suggestions on the manuscript. This research was

supported by the U.S. Department of Energy (DOE) Office of Energy Efficiency and Renewable Energy, Foundational Program to Advance Cell Efficiency (F-PACE), (C. L., Y. L. W., W. J. Y., N. P., M. A. J., Y. Y., S. J. P.), the Office of Basic Energy Sciences (BES), Materials Science and Engineering Division (A. R. L.), the U.S. DOE Grant No. DE-FG02-09ER46554 (T. J. P.), and by the BES Scientific User Facilities Division Shared Research Equipment (SHaRE) User Program (D. N. L.) at Oak Ridge National Laboratory. This research used resources of the National Energy Research Scientific Computing Center, which is supported by the DOE Office of Science under Contract No. DE-AC02-05CH11231.

*Now at SuperSTEM Facility, Daresbury, United Kingdom.
†Corresponding author.
pennycooksj@ornl.gov

[1] J. Britt and C. Ferekides, Appl. Phys. Lett. **62**, 2851 (1993).
[2] R. W. Birkmire and B. E. McCandless, Curr. Opin. Solid State Mater. Sci. **14**, 139 (2010).
[3] W. Shockley and H. J. Queisser, J. Appl. Phys. **32**, 510 (1961).
[4] M. A. Green, Prog. Photovoltaics **20**, 472 (2012).
[5] X. Wu, J. C. Keane, R. G. Dhere, C. Dehart, A. Duda, T. A. Gessert, S. Asher, D. H. Levi, and P. Shelton, *Proceedings of the 17th European Photovoltaic Solar Energy Conference* (WIP Munic/ETA Florence, Germany/Italy, 2001), p. 995.
[6] M. A. Green, K. Emery, Y. Hishikawa, W. Warta, and E. D. Dunlop, Prog. Photovoltaics **21**, 1 (2013).
[7] M. A. Green, K. Emery, Y. Hishikawa, W. Warta, and E. D. Dunlop, Prog. Photovoltaics **20**, 606 (2012).
[8] National Renewable Energy Laboratory, Best Research-Cell Efficiencies, http://www.nrel.gov/ncpv/images/efficiency_chart.jpg.
[9] A. McEvoy, T. Markvart, and L. Castaner, *Practical Handbook of Photovoltaics: Fundamentals and Applications: Fundamentals and Applications* (Elsevier Science, New York, 2003).
[10] G. Beaucarne, S. Bourdais, A. Slaoui, and J. Poortmans, Appl. Phys. A **79**, 469 (2004).
[11] I. Visoly-Fisher, S. R. Cohen, A. Ruzin, and D. Cahen, Adv. Mater. **16**, 879 (2004).
[12] I. Visoly-Fisher, S. R. Cohen, and D. Cahen, Appl. Phys. Lett. **82**, 556 (2003).
[13] I. Visoly-Fisher, S. R. Cohen, K. Gartsman, A. Ruzin, and D. Cahen, Adv. Funct. Mater. **16**, 649 (2006).
[14] C. Persson and A. Zunger, Appl. Phys. Lett. **87**, 211904 (2005).
[15] C. Persson and A. Zunger, Phys. Rev. Lett. **91**, 266401 (2003).
[16] D. Abou-Ras, B. Schaffer, M. Schaffer, S. S. Schmidt, R. Caballero, and T. Unold, Phys. Rev. Lett. **108**, 075502 (2012).
[17] H. Mönig, Y. Smith, R. Caballero, C. A. Kaufmann, I. Lauermann, M. C. Lux-Steiner, and S. Sadewasser, Phys. Rev. Lett. **105**, 116802 (2010).
[18] Y. Yan, C. S. Jiang, R. Noufi, S.-H. Wei, H. R. Moutinho, and M. M. Al-Jassim, Phys. Rev. Lett. **99**, 235504 (2007).
[19] C.-S. Jiang, F. S. Hasoon, H. R. Moutinho, H. A. Al-Thani, M. J. Romero, and M. M. Al-Jassim, Appl. Phys. Lett. **82**, 127 (2003).
[20] C.-S. Jiang, R. Noufi, K. Ramanathan, J. A. AbuShama, H. R. Moutinho, and M. M. Al-Jassim, Appl. Phys. Lett. **85**, 2625 (2004).
[21] S. S. Schmidt, D. Abou-Ras, S. Sadewasser, W. Yin, C. Feng, and Y. Yan, Phys. Rev. Lett. **109**, 095506 (2012).
[22] J. B. Li, V. Chawla, and B. M. Clemens, Adv. Mater. **24**, 720 (2012).
[23] M. Hafemeister, S. Siebentritt, J. Albert, M. C. Lux-Steiner, and S. Sadewasser, Phys. Rev. Lett. **104**, 196602 (2010).
[24] T. L. Chu and S. S. Chu, Solid-State Electron. **38**, 533 (1995).
[25] Y. Yan, M. M. Al-Jassim, and T. Demuth, J. Appl. Phys. **90**, 3952 (2001).
[26] J. R. Chelikowsky, Phys. Rev. Lett. **49**, 1569 (1982).
[27] J. F. Justo, A. Antonelli, and A. Fazzio, Solid State Commun. **118**, 651 (2001).
[28] S. P. Beckman and D. C. Chrzan, Physica (Amsterdam) **340–342**, 1001 (2003).
[29] P. Lu and D. J. Smith, Philos. Mag. B **62**, 435 (1990).
[30] S. J. Pennycook and D. E. Jesson, Phys. Rev. Lett. **64**, 938 (1990).
[31] S. J. Pennycook and D. E. Jesson, Ultramicroscopy **37**, 14 (1991).
[32] O. L. Krivanek, N. Dellby, and A. R. Lupini, Ultramicroscopy **78**, 1 (1999).
[33] A. Liechtenstein, V. I. Anisimov, and J. Zaanen, Phys. Rev. B **52**, R5467 (1995).
[34] V. I. Anisimov, J. Zaanen, and O. Andersen, Phys. Rev. B **44**, 943 (1991).
[35] S. L. Dudarev, G. A. Botton, S. Y. Savrasov, C. J. Humphreys, and A. P. Sutton, Phys. Rev. B **57**, 1505 (1998).
[36] Y. Wu, G. Chen, W. Yin, M. M. Al-Jassim, S. J. Pennycook, and Y. Yan (unpublished).
[37] P. E. Blöchl, Phys. Rev. B **50**, 17 953 (1994).
[38] G. Kresse and J. Furthmüller, Comput. Mater. Sci. **6**, 15 (1996).
[39] G. Kresse and J. Furthmüller, Phys. Rev. B **54**, 11 169 (1996).
[40] H. Hans Landolt, R. Bornstein, K. H. Hellwege, W. Freyland, M. Schulz, H. Weiss, and O. Madelung, *Landolt-Bornstein Numerical Data and Functional Relationships in Science and Technology. Group 3, Crystal and Solid State Physics*, (Springer, Berlin, 1982) Vol. 17b.
[41] G. Fonthal, L. Tirado-Mejia, J. Marin-Hurtado, H. Ariza-Calderon, and J. G. Mendoza-Alvarez, J. Phys. Chem. Solids **61**, 579 (2000).
[42] C. Li, J. Poplawsky, Y. Wu, A. R. Lupini, A. Mouti, D. N. Leonard, N. Paudel, K. Jones, W. Yin, M. Al-Jassim, Y. Yan, and S. J. Pennycook, [Ultramicroscopy (to be published)], http://dx.doi.org/10.1016/j.ultramic.2013.06.010.
[43] See Supplemental Material at http://link.aps.org/supplemental/10.1103/PhysRevLett.111.096403 for a movie showing the dislocation motion; and the band structure of an extrinsic stacking fault.
[44] J. Lee, W. Zhou, S. J. Pennycook, J. C. Idrobo, and S. T. Pantelides, Nat. Commun. **4**, 1650 (2013).
[45] D. Azulay, I. Balberg, and O. Millo, Phys. Rev. Lett. **108**, 076603 (2012).
[46] K. Taretto and U. Rau, J. Appl. Phys. **103**, 094523 (2008).